Current-Induced Spin-Orbit Torque and Field-Free Switching in Mo-Based Magnetic Heterostructures

Tian-Yue Chen,[1] Hsin-I Chan,[1] Wei-Bang Liao,[1] and Chi-Feng Pai[1,2,*]

[1]*Department of Materials Science and Engineering, National Taiwan University, Taipei 10617, Taiwan*
[2]*Center of Atomic Initiative for New Materials, National Taiwan University, Taipei 10617, Taiwan*

Magnetic heterostructure Mo/Co-Fe-B/MgO has strong perpendicular magnetic anisotropy and thermal stability. Through current-induced hysteresis loop shift measurements, we show that the damping-like spin-orbit torque (SOT) efficiency of Mo/Co-Fe-B/MgO heterostructures is $\xi_{DL} \approx -0.003 \pm 0.001$ and is fairly independent of the annealing temperature from 300 °C to 400 °C. Although $|\xi_{DL}|$ is small compared to those from Ta- or W-based heterostructures, reversible current-induced SOT switching of a thermally stable Mo/Co-Fe-B/MgO heterostruture can still be achieved. Furthermore, we observe field-free current-induced switching from a Mo/Co-Fe-B/MgO structure with the Mo layer being wedge-deposited. Our results indicate that even for a weak spin-orbit interaction 4*d* transition metal such as Mo, it is still possible to generate sufficient spin current for conventional SOT switching and to realize field-free current-induced switching by structural engineering.

I. INTRODUCTION

In the development of contemporary spin-transfer torque magnetoresistive random access memory (STT MRAM), perpendicular magnetic tunnel junction (PMTJ) is an essential device element, which has a better scalability and thermal stability when compared to its in-plane magnetized predecessor [1]. Among many magnetic heterostructures that can give rise to the perpendicular magnetic anisotropy (PMA), Ta/Co-Fe-B/MgO trilayer is one of the most studied and widely employed structures due to its simplicity and its compatibility with high tunneling magnetoresistance MgO junctions [2,3]. More importantly, not only for PMTJ and current-perpendicular-to-plane STT MRAM applications, Ta/Co-Fe-B/MgO heterostructure has also been shown to have significant spin-orbit torque (SOT) efficiency, which can be utilized for SOT-induced magnetic switching [4] and microwave generation [5] with the current-in-plane scheme. The heavy transition metal (HM)/Co-Fe-B/MgO PMA heterostructures, with HM = Ta, W [4,6,7], or Pt [8] (materials with large spin-Hall effects [9,10]), have become standard heterostructures for SOT studies. Characterizing the SOT efficiencies from various HM/Co-Fe-B/MgO structures, therefore, can provide valuable information for building more energy-efficient SOT MRAM devices.

On the other hand, enhancing the thermal stability of the magnetic memory element, which is the ferromagnetic Co-Fe-B layer in HM/Co-Fe-B/MgO heterostructures,

plays a critical role in achieving stable STT MRAM or SOT MRAM devices. Besides Ta, several other HM materials have also been demonstrated to be suitable buffer layers for enhancing the PMA in HM/Co-Fe-B/MgO structures. For instance, thermally annealed Hf/Co-Fe-B/MgO [11] and Mo/Co-Fe-B/MgO [12,13] have both been shown to gain greater PMA energy densities when compared to that of Ta/Co-Fe-B/MgO. Surprisingly, Mo/Co-Fe-B/MgO heterostructure can survive thermal annealing up to 450 °C, which makes it an attractive candidate for replacing Ta as the standard PMTJ buffer layer structure that can be compatible with modern CMOS processing [12–15]. Although Mo has been introduced as a PMA-enhancing insertion layer for a SOT study published by Wu *et al.* [16], its own SOT properties from a Mo/Co-Fe-B/MgO structure without other HM underlayers have yet to be reported.

In this work, we perform characterizations on the magnetic properties and the damping-like SOT (DL SOT) efficiencies from Mo/Co-Fe-B/MgO heterostructures with different annealing temperatures. We show that the DL SOT efficiency originating from a thermally annealed Mo/Co-Fe-B/MgO heterostructure with PMA is $|\xi_{DL}| = 0.003 \pm 0.001$ with the sign being negative, which is consistent with previous reports on the spin Hall angle of Mo [17–19]. The DL SOT efficiency of Mo/Co-Fe-B/MgO is also found to be independent of the annealing temperature within the range from 300 °C to 400 °C. By assuming that the observed SOT originates from the spin Hall effect (SHE) of Mo and a 100% spin transparency at the Mo/Co-Fe-B interface, we

*cfpai@ntu.edu.tw

estimate the lower bound of Mo spin Hall conductivity to be $|\sigma_{SH}| \approx 35(\hbar/e)\Omega^{-1}$ cm^{-1}. Although $|\xi_{DL}| \approx 0.003$ of the Mo-based structure is much smaller than those from Ta- or W-based magnetic heterostructures ($|\xi_{DL}| \geq 0.10$), we can still observe reversible current-induced SOT switching in micron-sized Mo/Co-Fe-B/MgO devices when an in-plane field is applied. More importantly, we show that if the Mo layer is wedge deposited, then an out-of-plane current-induced effective field will emerge even in the absence of an in-plane bias field. Pure current-induced magnetization switching can, therefore, be realized in Mo(wedge)/Co-Fe-B/MgO heterostructures. Our results suggest that although the strength of the current-induced SOT is small in Mo/Co-Fe-B/MgO heterostructures, it is not entirely negligible. In addition, by controlling the deposition method, it is possible to achieve field-free current-induced magnetization switching in HM/Co-Fe-B/MgO PMA structures even if the HM is a 4d transition metal with weak spin-orbit interaction.

II. MAGNETIC PROPERTIES CHARACTERIZATION

To characterize the magnetic properties of Mo/Co-Fe-B/MgO heterostructures, we prepare a series of Mo(4)/Co$_{40}$Fe$_{40}$B$_{20}$($t_{Co-Fe-B}$)/MgO(2)/Ta(2) on a thermally-oxidized silicon substrate by high-vacuum magnetron sputtering. Numbers in parentheses represent the nominal sputtered thickness of each layer and the Ta(2) serves as a capping layer to prevent oxidation. The base pressure of

the deposition system is approximately 3×10^{-8} Torr and the Ar working pressures for sputtering metallic and oxide layers are set to be 3 and 10 mTorr, respectively. After depositions, the films are annealed in vacuum at 300 °C for 1 h to induce PMA. A representative out-of-plane hysteresis loop obtained by magneto-optical Kerr effect (MOKE) from a Mo(4)/Co$_{40}$Fe$_{40}$B$_{20}$(1.4)/MgO(2)/Ta(2) film annealed at 300 °C is shown in Fig. 1(a), from which the PMA of the film is verified. We further characterize saturation magnetization M_s and effective anisotropy energy density K_{eff} of the annealed Mo/Co-Fe-B/MgO heterostructures by vibrating sample magnetometer (VSM), as shown in Figs. 1(b) and 1(c). The effective saturation magnetization is found to be $M_s = 1200$ emu/cm^3 with a magnetic dead layer of $t_{dead} = 0.8$ nm. The large magnetic dead layer might originate from the intermixing of Co-Fe-B and a buffer layer at the Mo/Co-Fe-B interface [20] or partial oxidation or boron segregation at the Co-Fe-B/MgO interface [21,22]. The $K_{eff}t_{Co-Fe-B}^{eff}$ vs $t_{Co-Fe-B}^{eff}$ ($= t_{Co-Fe-B} - t_{dead}$) plot also indicates that PMA exists when 0.4 nm $\leq t_{Co-Fe-B}^{eff} \leq 0.9$ nm (1.2 nm $\leq t_{Co-Fe-B} \leq 1.7$ nm), although the maximum $K_{eff}t_{Co-Fe-B}^{eff}$ value of 0.03 erg/cm^2 is smaller than that reported by Liu *et al.* [12] due to the existence of a magnetic dead layer. Next, we fix the nominal Co-Fe-B thickness at $t_{Co-Fe-B} = 1.4$ nm and study the dependence of Mo(4)/Co-Fe-B(1.4)/MgO(2) PMA on annealing temperature. As shown in Fig. 1(d), PMA of Mo(4)/Co-Fe-B(1.4)/MgO(2) exists for annealing temperature T_a ranges from 280 °C to 420 °C and the
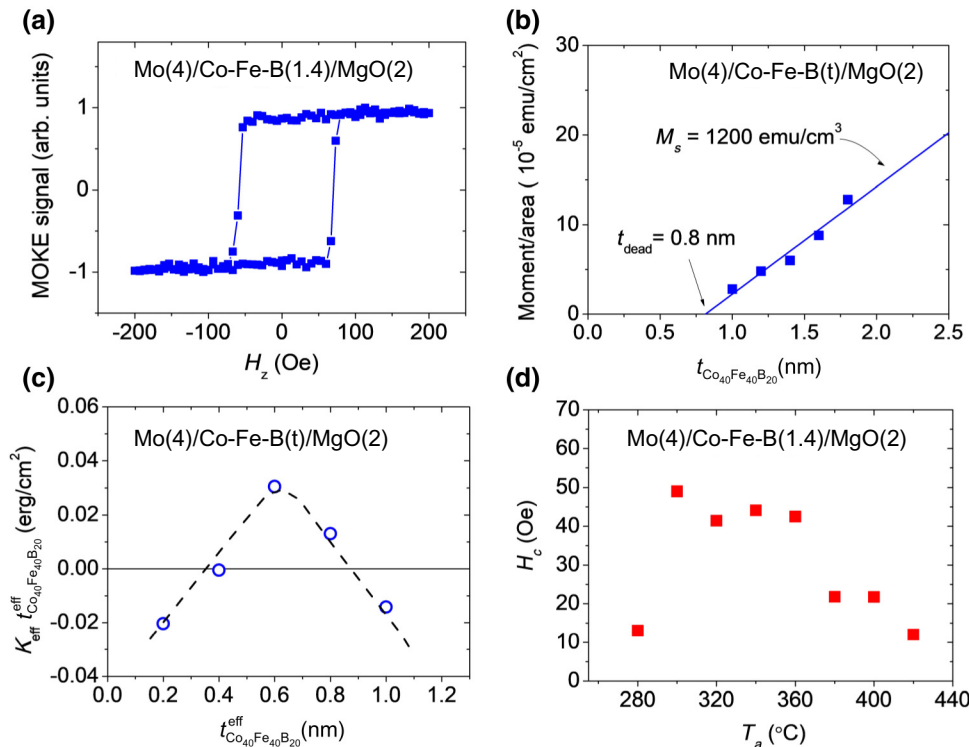

FIG. 1. (a) Representative out-of-plane hysteresis loop of a Mo(4)/Co-Fe-B(1.4)/MgO(2) film annealed at 300 °C. (b) Magnetic moment per area as a function of Co-Fe-B thickness $t_{Co-Fe-B}^{eff}$ for Mo(4)/Co-Fe-B($t_{Co-Fe-B}$)/MgO(2) films annealed at 300 °C. The line represents a linear fit to the data. (c) The product of effective magnetic anisotropy energy density and effective Co-Fe-B thickness as a function of effective Co-Fe-B thickness $t_{Co-Fe-B}^{eff}$ for Mo(4)/Co-Fe-B($t_{Co-Fe-B}$)/MgO(2) films annealed at 300 °C. The dashed line serves as guide to the eye. (d) Out-of-plane coercive field of Mo(4)/Co-Fe-B(1.4)/MgO(2) samples as a function of annealing temperature T_a.
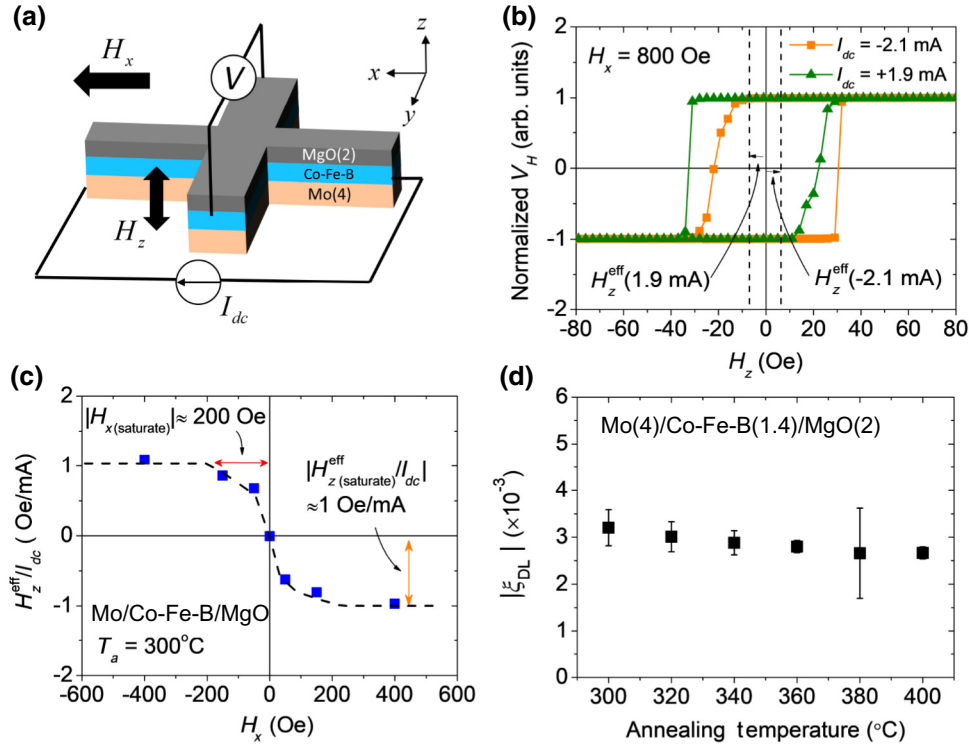
FIG. 2. (a) Schematic illustration of patterned Mo/Co-Fe-B/MgO Hall-bar structure and setup for current-induced hysteresis loop shift measurement. H_x and H_z stand for externally-applied in-plane and out-of-plane fields, respectively. I_{dc} represents the applied dc current. (b) Representative hysteresis loops obtained from a Mo(4)/Co-Fe-B(1.4)/MgO(2) Hall-bar sample (annealed at 300 °C) through an anomalous Hall effect with different I_{dc} and in-plane bias field $H_x = 800$ Oe. H_z^{eff} represents the effective field stemming from DL SOT. (c) H_z^{eff}/I_{dc} as a function of in-plane bias field H_x. (d) The estimated magnitude of DL SOT efficiency $|\xi_{DL}|$ for Mo(4)/Co-Fe-B(1.4)/MgO(2) samples as a function of annealing temperature T_a.

out-of-plane coercive field peaks at around $T_a \approx 300°$C. Therefore, we confirm that Mo/Co-Fe-B/MgO heterostructures can survive thermal annealing with T_a greater than 400 °C, which is consistent with previous reports.

III. DL SOT EFFICIENCY CHARACTERIZATION

After verifying the existence of PMA in Mo/Co-Fe-B/MgO structures over a wide range of annealing temperatures, we pattern a Mo(4)/Co-Fe-B(1.4)/MgO(2) film ($T_a = 300$ °C) into micron-sized Hall-bar devices through photolithography. The nominal width of the Hall-bar is $w = 5$ μm. In order to estimate the SOT efficiency from these devices, we utilize current-induced hysteresis loop shift measurement to quantify the out-of-plane effective field H_z^{eff}, which is a manifestation of the DL SOT acting on the chiral domain wall moments of the Co-Fe-B layer [8,23–27]. As schematically shown in Fig. 2(a), the Hall-bar device is subject to a static in-plane bias field H_x to overcome the effective field H_{DMI} that originates from Dzyaloshinski-Moriya interaction (DMI). While increasing the magnitude of H_x, the DMI-caused Néel-type chiral domain wall moments in the Co-Fe-B layer will gradually align with respect to H_x and further facilitate DL SOT-driven domain wall motion [28–30]. Once H_{DMI} is overcome, the full strength of DL SOT can be detected by the shift of out-of-plane hysteresis loops, which are recorded through anomalous Hall effect (AHE) from the Hall-bar device. Representative loop shift

results are shown in Fig. 2(b). A current-induced effective field H_z^{eff}, which is proportional to the strength of DL SOT, can be observed when $H_x = 800$ Oe is applied with a constant supply of dc current I_{dc}. The asymmetry of $\pm I_{dc}$ shown in Fig. 2(b) is to avoid measuring AHE loops with $I_{dc} = 0$ mA while stepping down the applied current by 0.4 mA. As shown in Fig. 2(c), the ratio of H_z^{eff}/I_{dc} saturates at around ± 1 Oe/mA when the in-plane bias field $H_x \approx \pm 200$ Oe. This suggests that $|H_{DMI}| \approx 200$ Oe and the DMI constant $|D| = \mu_0 M_s \delta |H_{DMI}| \approx 0.35$ mJ/m^2 [31], where the domain wall width δ is estimated by $\delta = \sqrt{A/K_{eff}}$ and the exchange stiffness constant A is assumed to be approximately 10^{-11} J/m. The magnitude of DMI for Mo/Co-Fe-B is, therefore, smaller than the reported values of 0.6–2.9 mJ/m^2 for large DMI Pt/Co [8,32–35], which indicates that Mo has a weaker spin-orbit coupling compared to Pt.

The saturated DL SOT efficiency ξ_{DL} of this Mo(4)/Co-Fe-B(1.4)/MgO(2) Hall-bar device can be further estimated by [36]

$$\xi_{DL} = \frac{2e}{\hbar} \left(\frac{2}{\pi} \right) \mu_0 M_s t_{Co-Fe-B}^{eff} w t_{Mo}$$
$$\left(\frac{\rho_{Co-Fe-B} t_{Mo} + \rho_{Mo} t_{Co-Fe-B}}{\rho_{Co-Fe-B} t_{Mo}} \right) \left(\frac{H_z^{eff}}{I_{dc}} \right), \quad (1)$$

where $\rho_{Co-Fe-B} = 180$ $\mu\Omega$ cm and $\rho_{Mo} = 85$ $\mu\Omega$ cm are the resistivities of the Co-Fe-B layer and Mo layer, respectively. The resistivities are determined by measuring the resistances of Mo/Co-Fe-B/MgO heterostructures with
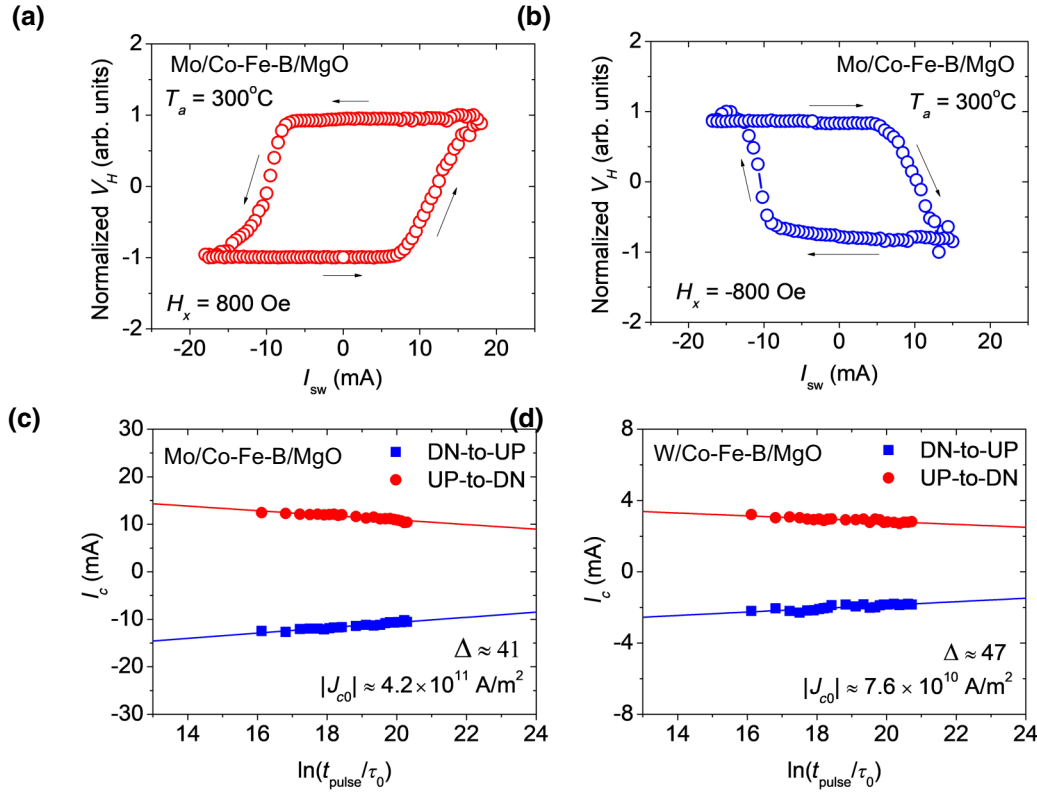
(a)

(b)

(c)

(d)

FIG. 3. (a),(b) Pulse current-induced switching of a 10-μm- wide Mo (4)/Co-Fe-B(1.4)/MgO(2) Hall-bar sample annealed at 300 °C with in-plane bias field $H_x = \pm 800$ Oe. The arrows indicate the switching directions. The applied current pulse width t_{pulse} dependence of critical switching current I_c for the (c) Mo(4)/Co-Fe-B(1.4)/MgO(2) and (d) W(4)/Co-Fe-B(1.4)/MgO (2) Hall-bar samples. Both are annealed at 300 °C. The solid lines represent linear fits to the experimental data.

various Mo layer thicknesses. Using the VSM-determined $M_s = 1200$ emu/cm^3 (SI unit 1.2×10^6 A/m), $t_{\text{Co-Fe-B}}^{\text{eff}} = 0.6$ nm, and the loop-shift-determined $H_z^{\text{eff}}/I_{\text{dc}} \approx -1$ Oe/ mA, the DL SOT efficiency is estimated to be $\xi_{\text{DL}} \approx -0.003$. This $|\xi_{\text{DL}}| \approx 0.003$ is the lower bound of the intrinsic spin Hall ratio of Mo due to (1) imperfect spin transmission at the HM/Co-Fe-B interface [37,38] and (2) possible current shunting in the Hall-bar device structure [39,40], which typically leads to an underestimation of the DL SOT efficiency. The lower bound of Mo spin Hall conductivity is, therefore, calculated to be $|\sigma_{\text{SH}}| \geq |\xi_{\text{DL}}/\rho_{\text{Mo}}| \approx 35(\hbar/e)\Omega^{-1}$ cm^{-1}. More importantly, the estimated DL SOT efficiency $|\xi_{\text{DL}}|$ of the Mo(4)/Co-Fe-B(1.4)/MgO(2) heterostructure is fairly independent of the annealing temperature 300 °C $\leq T_a \leq$ 400 °C, as summarized in Fig. 2(d). The T_a-independent $|\xi_{\text{DL}}| = 0.003 \pm 0.001$ of the Mo/ Co-Fe-B/MgO system suggests that Mo is a thermally stable buffer layer for studying both PMA and SOT for a wide range of annealing temperatures.

IV. CURRENT-INDUCED DL SOT SWITCHING

Although the DL SOT efficiency from Mo-based magnetic heterostructures is two orders of magnitude smaller than those from Pt-, Ta-, and W-based magnetic heterostructures [4,6,41,42], it is still possible to realize current-induced switching. To demonstrate SOT-driven magnetization switching, we apply current pulses

with pulse widths 0.01 s $\leq t_{pulse} \leq$ 1 s. Current-induced switching results recorded from a 10-μm-wide, 300 °C-annealed Mo(4)/Co-Fe-B(1.4)/MgO(2) Hall-bar device with $t_{pulse} = 0.1$ s and critical switching current $|I_c| \approx$ 10 mA are shown in Figs. 3(a) and 3(b). The opposite switching polarity with respect to the applied in-plane field $H_x = \pm 800$ Oe is consistent with the symmetry of SOT-driven dynamics [4,29,42]. Since SOT-driven magnetization switching is a thermally-activated process, I_c should depend on the applied current pulse width and can be expressed as [43]

$$I_c = I_{c0} \left[1 - \frac{1}{\Delta} \ln \left(\frac{t_{pulse}}{\tau_0} \right) \right], \quad (2)$$

where I_{c0} is the zero-thermal critical switching current, $\Delta \equiv U/k_B T$ is the thermal stability factor (U is the energy barrier), and $1/\tau_0 \approx 1$ GHz ($\tau_0 \approx 1$ ns) is the attempt rate for thermally-activated switching [44]. As shown in Fig. 3(c), linear trends can be found in the experimental I_c vs $\ln(t_{pulse}/\tau_0)$ plot. By performing linear fits of the switching data with Eq. (2), we estimate $|I_{c0}| \approx 20$ mA and $\Delta \approx 41$ for this Mo(4)/Co-Fe-B(1.4)/MgO(2) Hall-bar device. The zero-thermal critical switching current density is further calculated to be $|J_{c0}| \approx 4.2 \times 10^{11}$ A/m^2. By comparison, as shown in Fig. 3(d), the results from a W(4)/Co-Fe-B(1.4)/MgO(2) control sample indicate a similar thermal stability to Mo(4)/Co-Fe-B(1.4)/MgO(2),

but a much lower critical switching current density $|J_{c0}| \approx 7.6 \times 10^{10}$ A/m^2 due to the greater SHE from W [6,7].

V. FIELD-FREE CURRENT-INDUCED SWITCHING

Beyond conventional SOT switching of perpendicular magnetization, which typically requires an in-plane bias field, there has been an increasing interest to realize current-induced switching in the absence of an external field [45–50]. Although the origin of current-induced out-of-plane effective field H_z^{eff} is still elusive, it has been shown that by introducing a wedge structure in the oxide layer of the Ta/Co-Fe-B/TaO$_x$ system, such an effective field can be utilized to switch magnetization deterministically without applying any in-plane field [51,52]. A similar mysterious H_z^{eff} has also recently been seen in a Pt/W/Co-Fe-B/MgO heterostructure [53], which was attributed to the competing spin currents from the Pt and W buffer layers. Interestingly, the W layer in Ref. [53] is also obliquely deposited. To unveil the main cause of wedge-structure-induced H_z^{eff} and to understand if strong spin-orbit interaction materials are indeed necessary, we perform DL SOT efficiency characterizations for two Mo-based samples: Ta(2)/MgO(2)/Co-Fe-B(1.4)/Mo(10) and Ta(2)/MgO(2)/Co-Fe-B(1.4)/Mo(wedge). Wedge deposition is done by turning off the sample holder rotation during the sputtering of the

Mo layer, and the nominal thickness of Mo at the center of the film is approximately 7 nm. Both samples are annealed at 300 °C for 1 h to induce PMA and are patterned into Hall-bar devices with $w = 5$ μm. The layer structure and thickness gradient of the wedge-deposited sample and its relative orientation to the applied current/field during measurement are shown in Fig. 4(a). Note that we prepare the film in reverse order (MgO/Co-Fe-B/HM) to make sure the MgO and Co-Fe-B layers are flat with respect to the substrate and only the Mo layer is wedged. The magnetic dead layer thickness is determined to be $t_{\text{dead}} = 0.3$ nm by VSM measurements.

In Fig. 4(b), we summarize the measured $H_z^{\text{eff}}/I_{\text{dc}}$ for both uniform and wedge-deposited samples under different in-plane bias fields H_x through current-induced loop shift measurements. Although the overall H_x dependences of $H_z^{\text{eff}}/I_{\text{dc}}$ for both samples are similar, it is found that there exists a finite $H_z^{\text{eff}}/I_{\text{dc}} \approx 0.5$ Oe/mA at $H_x = 0$ Oe for the wedge-deposited device. In contrast, $H_z^{\text{eff}}/I_{\text{dc}} \leq 0.2$ Oe/mA for the uniform case when the in-plane field is absent. Note that the measured $|H_z^{\text{eff}}/I_{\text{dc}}|$ becomes smaller when the applied $H_x \geq 400$ Oe. It is possible that if the applied $|H_x|$ is much greater than $|H_{\text{DMI}}|$, then the magnetic moments in the film become more single-domain-like, and therefore, the SOT-driven or SOT-assisted domain nucleation/propagation is not as efficient as the intermediate H_x case. This slight decrease of DL SOT efficiency at
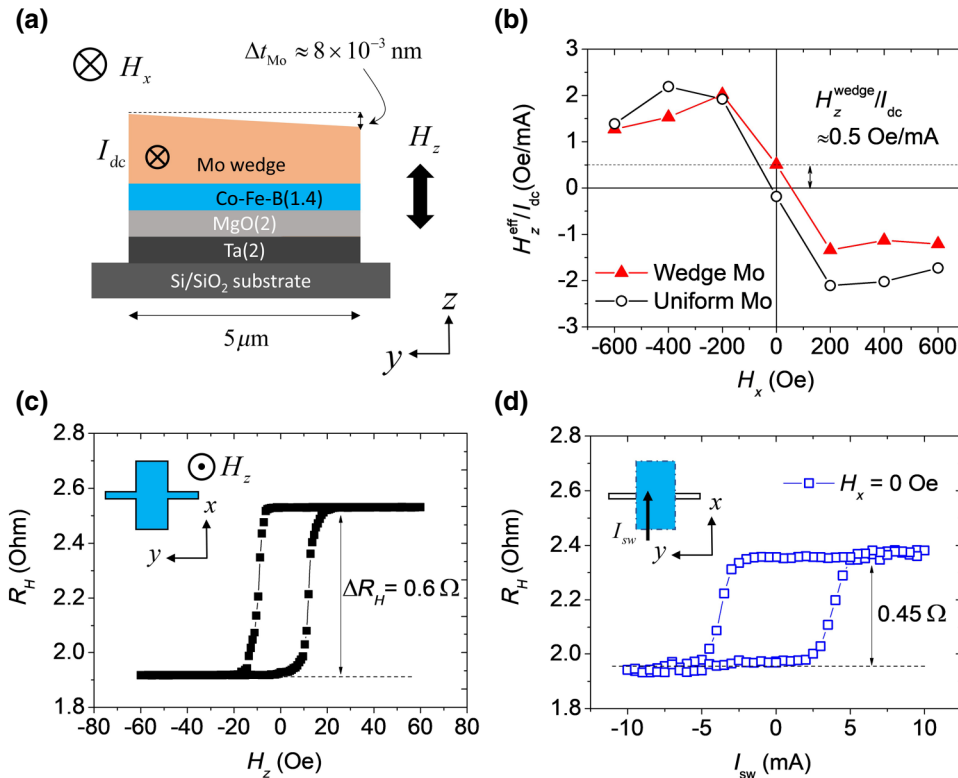

(a)

(b)

(c)

(d)

FIG. 4. (a) Layer structure of the wedge-deposited Mo sample (not to scale). (b) $H_z^{\text{eff}}/I_{\text{dc}}$ as functions of in-plane bias field H_x for uniform Mo (black circles) and wedge-deposited Mo (red triangles) Hall-bar samples. $H_z^{\text{wedge}}/I_{\text{dc}}$ represents the effective field per current that originates from the wedge structure. (c) Out-of-plane hysteresis loop and (d) field-free current-driven magnetization switching loop of a MgO(2)/Co-Fe-B(1.4)/Mo (wedge) Hall-bar device obtained via anomalous Hall effect. The Hall-bar top view illustrations indicate the area of magnetization being switched for each case.

$|H_x| \gg |H_{\mathrm{DMI}}|$ has also been seen in some recent works [54,55].

Due to the existence of a finite current-induced H_z^{eff} at $H_x = 0$ Oe in the wedge-deposited Mo device, deterministic current-induced magnetization can be achieved, although Mo is a transition metal with weak spin-orbit interaction. As shown in Fig. 4(c), the representative AHE result indicates that the MgO(2)/Co-Fe-B(1.4)/Mo(wedge) Hall-bar device has an overall Hall resistance difference of $\Delta R_H = 0.6\,\Omega$ for full magnetization switching. We observe a reversible and robust field-free current-induced magnetization switching of $\Delta R_H = 0.45\,\Omega$ from the very same wedge Mo device with $I_{\mathrm{sw}} \approx \pm 3.8$ mA, as shown in Fig. 4(d). The difference of ΔR_H between field-induced and current-induced switching is due to the device area that cannot be switched by current, as indicated by the insets of Figs. 4(c) and 4(d). The field-free switching of the wedge Mo device is performed on a probe station without electromagnets, which prevents the influence of remnant fields from magnetic pole pieces. We observe no field-free current-induced magnetization switching in the MgO/Co-Fe-B/Mo devices prepared by uniform deposition. Our results suggest that as long as the HM layer is deposited in an oblique way, there exists a non-negligible current-induced H_z^{eff} that can be employed to realize field-free switching. The HM layer is not necessarily being materials with significant spin-orbit interaction or SHE, such as Ta, W, or Pt.

Although conventional current-induced torques from strong spin-orbit interactions might not play important roles for the observed field-free switching in Mo-based devices, the Oersted field might play a crucial role. It has been shown that a current-induced Oersted field has a non-negligible z component at the edges of a Hall-bar sample [56], which will further create a longitudinal domain wall in some cases [57]. It has also been shown by simulations that an effective out-of-plane field will be created by the magnetic anisotropy gradient, which can be utilized to drive domain wall motion [58,59]. Therefore, we postulate that the current that we apply will first create a longitudinal domain wall in the sample, and then the magnetization switching will be achieved by lateral domain wall motion, which is driven by the transverse magnetic anisotropy gradient.

The oblique deposition or the glancing angle deposition (GLAD) of the Mo layer might also favor a tilted columnar microstructure [60,61], which modifies the Mo crystal structure symmetry. It is, therefore, possible that an extra damping-like SOT will be generated when applying current along a low-symmetry axis of Mo, which is similar to the phenomenon reported in a recent study on a WTe$_2$/Py system [62]. We hope future works that involve detailed MOKE imaging and microstructure analysis can further elucidate the real microscopic origin of wedge-direction-dependence field-free switching.

VI. CONCLUSION

To conclude, we show that a Mo/Co-Fe-B/MgO magnetic heterostructure has decent PMA, which is robust against thermal annealing within a temperature range of $280\,^{\circ}\mathrm{C} \le T_a \le 420\,^{\circ}\mathrm{C}$. The DL SOT efficiency in such a system is estimated to be small, but also fairly independent of the annealing temperature ($300\,^{\circ}\mathrm{C} \le T_a \le 400\,^{\circ}\mathrm{C}$), $|\xi_{\mathrm{DL}}| = 0.003 \pm 0.001$. The lower bound of spin Hall conductivity of Mo, $|\sigma_{\mathrm{SH}}| \approx 35(\hbar/e)\Omega^{-1}\,\mathrm{cm}^{-1}$, is, therefore, small when compared to other strong SHE metals such as Pt, Ta, and W. Despite the weak spin-orbit interaction of $4d$ transition metal Mo, conventional current-induced SOT switching can still be achieved in micron-sized Mo/Co-Fe-B/MgO Hall-bar devices with the aid of in-plane bias fields. Surprisingly, by depositing the Mo layer with an oblique angle, field-free current-induced magnetization switching can be realized. This discovery implies that strong spin-orbit interaction materials or spin Hall sources are not always necessary to achieve field-free current-induced switching, and "to wedge or not to wedge" during the thin-film deposition process is a more critical factor.

[1] B. Dieny, R. B. Goldfarb, and K. J. Lee, *Introduction to Magnetic Random-Access Memory* (Wiley IEEE Press, Hoboken, NJ, 2016).

[2] S. Ikeda, K. Miura, H. Yamamoto, K. Mizunuma, H. D. Gan, M. Endo, S. Kanai, J. Hayakawa, F. Matsukura, and H. Ohno, A perpendicular-anisotropy CoFeB-MgO magnetic tunnel junction, Nat. Mater. **9,** 721 (2010).

[3] D. C. Worledge, G. Hu, D. W. Abraham, J. Z. Sun, P. L. Trouilloud, J. Nowak, S. Brown, M. C. Gaidis, E. J. O'Sullivan, and R. P. Robertazzi, Spin torque switching of perpendicular Ta vertical bar CoFeB vertical bar MgO-based magnetic tunnel junctions, Appl. Phys. Lett. **98,** 022501 (2011).

[4] L. Q. Liu, C.-F. Pai, Y. Li, H. W. Tseng, D. C. Ralph, and R. A. Buhrman, Spin-torque switching with the giant spin Hall effect of tantalum, Science **336,** 555 (2012).

[5] L. Q. Liu, C.-F. Pai, D. C. Ralph, and R. A. Buhrman, Magnetic Oscillations Driven by the Spin Hall Effect in 3-Terminal Magnetic Tunnel Junction Devices, Phys. Rev. Lett. **109,** 186602 (2012).

[6] C.-F. Pai, L. Q. Liu, Y. Li, H. W. Tseng, D. C. Ralph, and R. A. Buhrman, Spin transfer torque devices utilizing the giant spin Hall effect of tungsten, Appl. Phys. Lett. **101,** 122404 (2012).

[7] Q. Hao and G. Xiao, Giant Spin Hall Effect and Switching Induced by Spin-Transfer Torque in a $W/Co_{40}Fe_{40}B_{20}/MgO$ Structure with Perpendicular Magnetic Anisotropy, Phys. Rev. Applied **3,** 034009 (2015).

[8] C. F. Pai, M. Mann, A. J. Tan, and G. S. D. Beach, Determination of spin torque efficiencies in heterostructures with perpendicular magnetic anisotropy, Phys. Rev. B **93,** 144409 (2016).

[9] A. Hoffmann, Spin Hall effects in metals, IEEE Trans. Magn. **49,** 5172 (2013).

[10] J. Sinova, S. O. Valenzuela, J. Wunderlich, C. H. Back, and T. Jungwirth, Spin Hall effects, Rev. Mod. Phys. **87,** 1213 (2015).

[11] T. Liu, J. W. Cai, and L. Sun, Large enhanced perpendicular magnetic anisotropy in CoFeB/MgO system with the typical Ta buffer replaced by an Hf layer, AIP Adv. **2,** 032151 (2012).

[12] T. Liu, Y. Zhang, J. W. Cai, and H. Y. Pan, Thermally robust Mo/CoFeB/MgO trilayers with strong perpendicular magnetic anisotropy, Sci. Rep. **4,** 05895 (2014).

[13] M. Li, J. Lu, G. Yu, X. Li, G. Han, X. Chen, H. Shi, G. Yu, P. K. Amiri, and K. L. Wang, Influence of inserted Mo layer on the thermal stability of perpendicularly magnetized $Ta/Mo/Co20Fe60B20/MgO/Ta$ films, AIP Adv. **6,** 045107 (2016).

[14] B. Fang, X. Zhang, S. Zhang, Z. M. Zeng, and J. W. Cai, Tunnel magnetoresistance in thermally robust Mo/CoFeB/MgO tunnel junction with perpendicular magnetic anisotropy, AIP Adv. **5,** 067116 (2015).

[15] K. Watanabe, S. Fukami, H. Sato, S. Ikeda, F. Matsukura, and H. Ohno, Annealing temperature dependence of magnetic properties of CoFeB/MgO stacks on different buffer layers, Jpn. J. Appl. Phys. **56,** 0802b2 (2017).

[16] D. Wu, G. Q. Yu, Q. M. Shao, X. Li, H. Wu, K. L. Wong, Z. Z. Zhang, X. F. Han, P. K. Amiri, and K. L. Wang, In-plane current-driven spin-orbit torque switching in perpendicularly magnetized films with enhanced thermal tolerance, Appl. Phys. Lett. **108,** 212406 (2016).

[17] M. Morota, K. Ohnishi, T. Kimura, and Y. Otani, Spin Hall effect in Molybdenum wires, J. Appl. Phys. **105,** 07C712 (2009).

[18] O. Mosendz, J. E. Pearson, F. Y. Fradin, G. E. W. Bauer, S. D. Bader, and A. Hoffmann, Quantifying Spin Hall Angles from Spin Pumping: Experiments and Theory, Phys. Rev. Lett. **104,** 046601 (2010).

[19] M. Morota, Y. Niimi, K. Ohnishi, D. H. Wei, T. Tanaka, H. Kontani, T. Kimura, and Y. Otani, Indication of intrinsic spin Hall effect in 4d and 5d transition metals, Phys. Rev. B **83,** 174405 (2011).

[20] M. Kowalewski, W. H. Butler, N. Moghadam, G. M. Stocks, T. C. Schulthess, K. J. Song, J. R. Thompson, A. S. Arrott, T. Zhu, J. Drewes, R. R. Katti, M. T. McClure, and O. Escorcia, The effect of Ta on the magnetic thickness of permalloy (Ni81Fe19) films, J. Appl. Phys. **87,** 5732 (2000).

[21] S. Pinitsoontorn, A. Cerezo, A. K. Petford-Long, D. Mauri, L. Folks, and M. J. Carey, Three-dimensional atom probe investigation of boron distribution in CoFeB/MgO/CoFeB magnetic tunnel junctions, Appl. Phys. Lett. **93,** 071901 (2008).

[22] C. Y. You, T. Ohkubo, Y. K. Takahashi, and K. Hono, Boron segregation in crystallized MgO/amorphous-Co40Fe40B20 thin films, J. Appl. Phys. **104,** 033517 (2008).

[23] K. Ueda, M. Mann, C.-F. Pai, A.-J. Tan, and G. S. D. Beach, Spin-orbit torques in Ta/TbxCo100-x ferrimagnetic alloy films with bulk perpendicular magnetic anisotropy, Appl. Phys. Lett. **109,** 232403 (2016).

[24] J. Finley and L. Liu, Spin-Orbit-Torque Efficiency in Compensated Ferrimagnetic Cobalt-Terbium Alloys, Phys. Rev. Applied **6,** 054001 (2016).

[25] R. Mishra, J. W. Yu, X. P. Qiu, M. Motapothula, T. Venkatesan, and H. Yang, Anomalous Current-Induced Spin Torques in Ferrimagnets near Compensation, Phys. Rev. Lett. **118,** 167201 (2017).

[26] J. H. Han, A. Richardella, S. A. Siddiqui, J. Finley, N. Samarth, and L. Q. Liu, Room-Temperature Spin-Orbit Torque Switching Induced by a Topological Insulator, Phys. Rev. Lett. **119,** 077702 (2017).

[27] I. Yuto, K. Masashi, L. Yong-Chang, N. Yoshinobu, and H. Masamitsu, Domain-wall resistance in CoFeB-based heterostructures with interface Dzyaloshinskii–Moriya interaction, Appl. Phys. Express **11,** 073001 (2018).

[28] S. Emori, U. Bauer, S. M. Ahn, E. Martinez, and G. S. D. Beach, Current-driven dynamics of chiral ferromagnetic domain walls, Nat. Mater. **12,** 611 (2013).

[29] O. J. Lee, L. Q. Liu, C. F. Pai, Y. Li, H. W. Tseng, P. G. Gowtham, J. P. Park, D. C. Ralph, and R. A. Buhrman, Central role of domain wall depinning for perpendicular magnetization switching driven by spin torque from the spin Hall effect, Phys. Rev. B **89,** 024418 (2014).

[30] S. Emori, E. Martinez, K. J. Lee, H. W. Lee, U. Bauer, S. M. Ahn, P. Agrawal, D. C. Bono, and G. S. D. Beach, Spin Hall torque magnetometry of Dzyaloshinskii domain walls, Phys. Rev. B **90,** 184427 (2014).

[31] A. Thiaville, S. Rohart, E. Jue, V. Cros, and A. Fert, Dynamics of Dzyaloshinskii domain walls in ultrathin magnetic films, Europhys. Lett. **100,** 57002 (2012).

[32] S. Pizzini, J. Vogel, S. Rohart, L. D. Buda-Prejbeanu, E. Jue, O. Boulle, I. M. Miron, C. K. Safeer, S. Auffret, G. Gaudin, and A. Thiaville, Chirality-Induced Asymmetric Magnetic Nucleation in Pt/Co/AlOx Ultrathin Microstructures, Phys. Rev. Lett. **113,** 047203 (2014).

[33] A. Hrabec, N. A. Porter, A. Wells, M. J. Benitez, G. Burnell, S. McVitie, D. McGrouther, T. A. Moore, and C. H. Marrows, Measuring and tailoring the Dzyaloshinskii-Moriya interaction in perpendicularly magnetized thin films, Phys. Rev. B **90,** 020402 (2014).

[34] C. Moreau-Luchaire, C. Moutafis, N. Reyren, J. Sampaio, C. A. F. Vaz, N. Van Horne, K. Bouzehouane, K. Garcia, C. Deranlot, P. Warnicke, P. Wohlhüter, J. M. George, M. Weigand, J. Raabe, V. Cros, and A. Fert, Additive interfacial chiral interaction in multilayers for stabilization of small individual skyrmions at room temperature, Nat. Nanotechnol. **11,** 444 (2016).

[35] P. Thai Ha, J. Vogel, J. Sampaio, M. Vaňatka, J. C. Rojas-Sánchez, M. Bonfim, D. S. Chaves, F. Choueikani, P. Ohresser, E. Otero, A. Thiaville, and S. Pizzini, Very large domain wall velocities in Pt/Co/GdOx and Pt/Co/Gd tri-layers with Dzyaloshinskii-Moriya interaction, Europhys. Lett. **113,** 67001 (2016).

[36] T. C. Wang, T. Y. Chen, H. W. Yen, and C. F. Pai, Comparative study on spin-orbit torque efficiencies from W/ferromagnetic and W/ferrimagnetic heterostructures, Phys. Rev. Mater. **2,** 014403 (2018).

[37] W. Zhang, W. Han, X. Jiang, S.-H. Yang, and S. S. P. Parkin, Role of transparency of platinum-ferromagnet interfaces in determining the intrinsic magnitude of the spin Hall effect, Nat. Phys. **11,** 496 (2015).

[38] C. F. Pai, Y. X. Ou, L. H. Vilela-Leao, D. C. Ralph, and R. A. Buhrman, Dependence of the efficiency of spin Hall torque on the transparency of Pt/ferromagnetic layer interfaces, Phys. Rev. B **92,** 064426 (2015).

[39] T. Y. Tsai, T. Y. Chen, C. T. Wu, H. I. Chan, and C. F. Pai, Spin-orbit torque magnetometry by wide-field magneto-optical Kerr effect, Sci. Rep. **8,** 5613 (2018).

[40] L. Neumann and M. Meinert, Influence of the Hall-bar geometry on harmonic Hall voltage measurements of spin-orbit torques, AIP Adv. 8, 095320 (2018)..

[41] L. Q. Liu, T. Moriyama, D. C. Ralph, and R. A. Buhrman, Spin-Torque Ferromagnetic Resonance Induced by the Spin Hall Effect, Phys. Rev. Lett. **106,** 036601 (2011).

[42] L. Q. Liu, O. J. Lee, T. J. Gudmundsen, D. C. Ralph, and R. A. Buhrman, Current-Induced Switching of Perpendicularly Magnetized Magnetic Layers Using Spin Torque from the Spin Hall Effect, Phys. Rev. Lett. **109,** 096602 (2012).

[43] R. H. Koch, J. A. Katine, and J. Z. Sun, Time-Resolved Reversal of Spin-Transfer Switching in a Nanomagnet, Phys. Rev. Lett. **92,** 088302 (2004).

[44] A. V. Khvalkovskiy, D. Apalkov, S. Watts, R. Chepulskii, R. S. Beach, A. Ong, X. Tang, A. Driskill-Smith, W. H. Butler, P. B. Visscher, D. Lottis, E. Chen, V. Nikitin, and M. Krounbi, Basic principles of STT-MRAM cell operation in memory arrays, J. Phys. D: Appl. Phys. **46,** 074001 (2013).

[45] S. Fukami, C. L. Zhang, S. DuttaGupta, A. Kurenkov, and H. Ohno, Magnetization switching by spin-orbit torque in an antiferromagnet-ferromagnet bilayer system, Nat. Mater. **15,** 535 (2016).

[46] Y. C. Lau, D. Betto, K. Rode, J. M. D. Coey, and P. Stamenov, Spin-orbit torque switching without an external field using interlayer exchange coupling, Nat. Nanotechnol. **11,** 758 (2016).

[47] Y. W. Oh, S. H. C. Baek, Y. M. Kim, H. Y. Lee, K. D. Lee, C. G. Yang, E. S. Park, K. S. Lee, K. W. Kim, G. Go, J. R. Jeong, B. C. Min, H. W. Lee, K. J. Lee, and B. G. Park, Field-free switching of perpendicular magnetization through spin-orbit torque in antiferromagnet/ferromagnet/oxide structures, Nat. Nanotechnol. **11,** 878 (2016).

[48] A. van den Brink, G. Vermijs, A. Solignac, J. Koo, J. T. Kohlhepp, H. J. M. Swagten, and B. Koopmans, Field-free magnetization reversal by spin-Hall effect and exchange bias, Nat. Commun. **7,** 10854 (2016).

[49] J.-Y. Chen, M.DC, D. Zhang, Z. Zhao, M. Li, and J.-P. Wang, Field-free spin-orbit torque switching of composite

[50] perpendicular CoFeB/Gd/CoFeB layers utilized for three-terminal magnetic tunnel junctions, Appl. Phys. Lett. **111,** 012402 (2017).

[50] K. M. Cai, M. Y. Yang, H. L. Ju, S. M. Wang, Y. Ji, B. H. Li, K. W. Edmonds, Y. Sheng, B. Zhang, N. Zhang, S. Liu, H. Z. Zheng, and K. Y. Wang, Electric field control of deterministic current-induced magnetization switching in a hybrid ferromagnetic/ferroelectric structure, Nat. Mater. **16,** 712 (2017).

[51] G. Q. Yu, L. T. Chang, M. Akyol, P. Upadhyaya, C. L. He, X. Li, K. L. Wong, P. K. Amiri, and K. L. Wang, Current-driven perpendicular magnetization switching in Ta/CoFeB/[TaOx or MgO/TaOx] films with lateral structural asymmetry, Appl. Phys. Lett. **105,** 102411 (2014).

[52] G. Q. Yu, P. Upadhyaya, Y. B. Fan, J. G. Alzate, W. J. Jiang, K. L. Wong, S. Takei, S. A. Bender, L. T. Chang, Y. Jiang, M. R. Lang, J. S. Tang, Y. Wang, Y. Tserkovnyak, P. K. Amiri, and K. L. Wang, Switching of perpendicular magnetization by spin-orbit torques in the absence of external magnetic fields, Nat. Nanotechnol. **9,** 548 (2014).

[53] Q. Ma, Y. Li, D. B. Gopman, Y. P. Kabanov, R. D. Shull, and C. L. Chien, Switching a Perpendicular Ferromagnetic Layer by Competing Spin Currents, Phys. Rev. Lett. **120,** 117703 (2018).

[54] J. Cao, Y. Chen, T. Jin, W. Gan, Y. Wang, Y. Zheng, H. Lv, S. Cardoso, D. Wei, and W. S. Lew, Spin orbit torques induced magnetization reversal through asymmetric domain wall propagation in Ta/CoFeB/MgO structures, Sci. Rep. **8,** 1355 (2018).

[55] M. Mann and G. S. D. Beach, Reduction of in-plane field required for spin-orbit torque magnetization reversal by insertion of Au spacer in Pt/Au/Co/Ni/Co/Ta, APL Mater. **5,** 106104 (2017).

[56] C. J. Durrant, R. J. Hicken, Q. Hao, and G. Xiao, Scanning Kerr microscopy study of current-induced switching in Ta/CoFeB/MgO films with perpendicular magnetic anisotropy, Phys. Rev. B **93,** 014414 (2016).

[57] D. Bhowmik, M. E. Nowakowski, L. You, O. Lee, D. Keating, M. Wong, J. Bokor, and S. Salahuddin, Deterministic domain wall motion orthogonal to current flow due to spin orbit torque, Sci. Rep. **5,** 11823 (2015).

[58] K. Yamada, S. Murayama, and Y. Nakatani, Magnetic domain wall motion in Co/Ni nanowires induced by a sloped electric field, Appl. Phys. Lett. **108,** 202405 (2016).

[59] Y. Zhang, S. Luo, X. Yang, and C. Yang, Spin-orbit-torque-induced magnetic domain wall motion in Ta/CoFe nanowires with sloped perpendicular magnetic anisotropy, Sci. Rep. **7,** 2047 (2017).

[60] T. G. Knorr and R. W. Hoffman, Dependence of geometric magnetic anisotropy in thin iron films, Phys. Rev. **113,** 1039 (1959).

[61] A. Barranco, A. Borras, A. R. Gonzalez-Elipe, and A. Palmero, Perspectives on oblique angle deposition of thin films: From fundamentals to devices, Prog. Mater. Sci. **76,** 59 (2016).

[62] D. MacNeill, G. M. Stiehl, M. H. D. Guimaraes, R. A. Buhrman, J. Park, and D. C. Ralph, Control of spin–orbit torques through crystal symmetry in WTe_2/ferromagnet bilayers, Nat. Phys. **13,** 300 (2016).